*J. Earth Syst. Sci.* (2021)130 100
https://doi.org/10.1007/s12040-021-01590-6



# Glass spherules from Antarctica blue ice and deep-sea sediment of the Central Indian Ocean Basin

D Fernandes[1,2,*], N G Rudraswami[1], M Pandey[1,2] and M Kotha[2]

[1]*National Institute of Oceanography (Council of Scientific and Industrial Research), Dona Paula, Goa 403 004, India.*
[2]*School of Earth, Ocean and Atmospheric Sciences, Goa University, Taleigao Plateau, Goa 403 206, India.*
**Corresponding author. e-mail: dafilgofernandes@gmail.com*

MS received 21 September 2020; revised 19 January 2021; accepted 26 January 2021

We report the chemical composition of 176 glass spherules obtained from Antarctica blue ice and deep-sea sediments from the Central Indian Ocean Basin. This study compares the chemistry of glass spherules collected from various reservoirs, thereby allowing us to look into possible bias and efficiency of different collection techniques. Glass spherules have experienced extreme heating among the S-type cosmic spherules, and have suffered significant ablative elemental loss for which their precursors remain ambiguous. The previous model calculation for the glass spherules indicates chemical changes due to atmospheric entry. In addition, the earlier heating experiment results for the glass spherules show some insight into their formation processes. We report Ca–Al glass spherules that have high $CaO+Al_2O_3$ >9 wt% indicating larger particles with excessive evaporation of moderately volatiles (Fe, Si, Mg) resulting in refractory (Ca, Al) enriched glass or equilibration of minor Ca and Al phases in glass. Glass spherules from Antarctica and deep-sea are morphologically distinct and happen to have ablated most of their elemental Fe during atmospheric entry, however despite it, their bulk chemical composition and atomic ratios indicate to have a broad correspondence with carbonaceous chondrites, thereby, preserving the precursor properties.

**Keywords.** Cosmic spherule; Antarctica; deep-sea; ablation; atmospheric entry.

## 1. Introduction

Cosmic spherules are melted extraterrestrial dust, that have been recovered from the surface of the Earth. Extraterrestrial matter that hits the upper atmosphere as dust is estimated to be near ∼40,000 ton/annum (Love and Brownlee 1991). Majority of this extraterrestrial dust reaching the Earth's surface is believed to have sourced mainly either from asteroid belt or cometary bodies (Bradley *et al.* 1988; Maurette *et al.* 1991; Brownlee *et al.* 1993; Taylor *et al.* 1998; Genge *et al.* 2008). One of the main reasons suspected for extraterrestrial dust to have asteroidal origin is the dynamic main asteroid belt that evolves due to collisions between asteroids generating dust that is injected into Earth's resonance orbit (Verniani 1969).

Supplementary material pertaining to this article is available on the *Journal of Earth System Science* website (http://www.ias.ac.in/Journals/Journal_of_Earth_System_Science).

Published online: 22 May 2021

Especially, some of the loose carbonaceous asteroids, which are agglomerates of porous rock, are more susceptible to generate dust (Gradie *et al.* 1989). The observations made from the zodiacal dust cloud that envelopes the asteroid belt have shown to oscillate its dust density randomly in time (Dermott *et al.* 1984). A large portion of these dust particles while moving towards the Sun, transit across the Earth's resonance orbit from which minor quantities get trapped and are later set in motion at higher altitudes due to gravitational focussing (Dohnanyi 1976; Flynn 1989; Rudraswami *et al.* 2016). Most of these dust particles in the process, due to frictional heating with the air molecules generate enough heat, that turns them into cosmic spherules before reaching the Earth's surface. In this respect, glass spherules turn out to be the most heated particles, but calcium-, aluminium-, and titanium-rich (CAT) spherules, being rich in refractory elements, have experienced the highest temperature (Taylor *et al.* 2000; Genge *et al.* 2008). The formation conditions and the precursors for both these spherules remain poorly defined. Significant modelling and experimental work performed in the past has strengthened our understanding of these spherules. Previous works, propose that glass spherules have witnessed nearly 20% of ablative loss (Taylor *et al.* 2000; Cordier *et al.* 2011; Rudraswami *et al.* 2012). These spherules are devoid of mineral phases, making them harder to understand and decipher their precursors. However, studies suggest that their primordial trend in elemental ratios remains intact (Brownlee *et al.* 1997; Taylor *et al.* 2000; Cordier *et al.* 2011) despite the intense loss of elements due to ablation and chemical changes by thermal alteration.

In this work, the emphasis is to provide the morphology and textural features observed in glass spherules from Antarctica and deep-sea sediments. These glasses have been inspected to identify the plausible bias pertaining to their collection technique. The environment and their chemical compositions are assessed to comprehend the changes glass spherules have undergone compared to the rest of the S-type spherules. We have combined minor and major elemental oxide studies in glass spherules to understand their content and compare elemental ratios with chondrites to identify their possible precursors. Furthermore, the details on elemental variation in glass spherules will improve our understanding of their heating process.

## 2. Sample collection and methodology

Samples for this study were collected from the deep-sea sediments of the Indian Ocean recovered from a water depth of ∼5200 m from the surface. The deep-sea sediments were extracted on various cruises onboard using Okean grab, that has a seafloor penetration depth of 15 cm and sediment carrying capacity of ∼50 kg sieved using ∼200 μm mesh size (Prasad *et al.* 2013). The age of the cosmic spherules was determined to be ∼50,000 years based on tektites (Prasad *et al.* 2013). The tektites related to Australasian impact event ∼0.77 Ma are widespread in the entire Indian Ocean region (Kunz *et al.* 1995; Prasad *et al.* 2007). Three sediment cores taken at the collection site were searched for microtektites belonging to this impact event. The terrestrial age for topmost sediments is estimated based on sedimentation rate and peak microtektites abundance in the sediment cores (Prasad *et al.* 2013).

The samples from Antarctica Indian Maitri station, Schirmacher Oasis, were obtained from melting the blue ice. Ice was extracted using basic tools and melted at the station in large clean vessels. Their subsequent meltwater was sieved using a sieve size of ∼50 μm (Rudraswami *et al.* 2018a, b; Rudraswami *et al.* 2020). This was later subjected to drying and magnetic separation. Although the total volume of ice melted was ∼50 tons, the glass spherules considered in this study are from 12 tons of samples.

All spherules were observed under a binocular microscope and individually handpicked. The picked samples were mounted on epoxy and polished to expose the surface area. The polished surfaces were coated with carbon and examined under a scanning electron microscope (SEM, JEOL JSM-IT300LV, and JSM-5800LV) equipped with an energy dispersive spectrometer detector (EDS, Aztec Energy EDS Microanalysis from Oxford instruments) for observing their textural features (Prasad *et al.* 2013; Rudraswami *et al.* 2018a, b). Glass spherules being devoid of mineral phases show plain textures in their backscattered electron images and were easy to sort from the rest of the stony spherules. The chemical composition of these glass spherules was obtained using Electron Probe Micro Analyzer (EPMA, Cameca SX5). The electron microprobe parameters set for generating the chemical composition include accelerating voltage of 15 kV, beam diameter of ∼5 μm and a beam current of 12 nA. Since glass spherules are

texturally homogeneous, multiple spots were analyzed at several places that were later averaged to obtain their bulk chemical composition.

## 3. Results

Antarctica micrometeorite (AMM) collection greatly dominates glass spherules ∼65%, compared to deep-sea sediments (DSS) that shows ∼35%. This may be due to the etching of the glass spherules that is quite common in deep-sea. These results are well consistent with the previous observations made from glass spherules of DSS that have etched rims (Blanchard *et al.* 1980; Brownlee *et al.* 1997; Genge *et al.* 2008; Prasad *et al.* 2013). It is quite interesting, that the glass spherule population from both these techniques show notable changes in their internal texture and morphology. Backscattered electron images for glass spherules from the AMM show perfectly round outlines and their cross-section interior feature homogeneous texture. Many of them have well-rounded cavities inside. However, results are quite different for glass spherules obtained by the magnetic separation method, which shows scalloped outlines (figure 1g, h). Reports about the DSS population described in earlier study have shown to contain considerable alteration rims with scalloped outgrowths (Brownlee *et al.* 1997; Rudraswami *et al.* 2012). Conversely, such glass spherules with scalloped features are hardly noted in the AMM population. These strongly suggest a possible bias that needs to be addressed. Although the only form of alteration observed in AMM glass spherules is palagonite-like in resemblance apparent in one or a few of the spherules (Van Ginneken *et al.* 2016) (figure 1d). Moreover, some glass spherules in the AMM, that consist of metal bead are normally oval and often display striated patterns (figure 1e). Other glass spherules, that contain small spherulitic centers inside, growth appears to control the shape of the host spherule (figure 1b, c, f). All these features correspond to the morphology of glass spherules and consequently imply disturbances in its development due to submicron crystal growth.

The size distribution of glass spherules shows a normal trend, shown in (figure 2a). AMM population is comparatively much smaller and its significant number concentrates between size ranges of 50–200 μm. In contrast, the DSS population is quantitatively lesser and constitutes only 62 spherules. Larger size for the DSS population is merely an artifact that is sieved using large-sized mesh, however, they are also much older (Prasad *et al.* 2013). Chemical composition for individual glass spherules has been provided in table 1 and supplementary data. Bulk chemical analyses for these glass spherules of different population are similar compared to those reported in earlier studies, thereby allow us to classify them as categorised in Cordier *et al.* (2011). Majority of the glass spherules belong to the normal group, having an oxide range of $SiO_2$ 34–57 wt%, MgO 20–49 wt%, FeO 7–37 wt%, CaO 0–4 wt%, and $Al_2O_3$ 0–6 wt%, (Ca+Al <9 wt%). The atomic ratios for normal glass show a range of Mg/Si 0.7–1.8, Fe/Si 0.1–0.9, and Ti/Si 0–0.006. Although, the FeO wt% in glass spherules from a normal group is variable, those spherules with scalloped outlines are relatively Fe enriched, which at the most are magnetic substrates. The minor oxide content for glass spherules constitutes; $Cr_2O_3$ 0–1.1 wt%, much lower in content apparent in significant glass spherules that may be due to volatile nature of $Cr_2O_3$ at higher temperatures, MnO ranges between 0.07 and 1.28 wt%, that is almost consistent with FeO wt%, $TiO_2$ 0–0.36 wt%, shows a fairly constant trend in most with an average of 0.12 wt% (figure 3a–c), other oxides like NiO within many glass spherules is negligible, but is found to go up to ∼1.8 wt%.

Additionally, three glass spherules analysed for their chemical composition closely resemble the Ca–Al group that exists only in AMM population that are different from CAT spherules (Taylor *et al.* 2000; Genge *et al.* 2008; Cordier *et al.* 2011). The Ca–Al spherules differ from the normal glass spherules and contain higher refractory oxides with maximum CaO up to ∼5 wt% and $Al_2O_3$ up to ∼14 wt% (table 1). These spherules have atomic ratios Fe/Si 0.31–0.40, Mg/Si 0.50–0.97, and Ti/Si 0.0007–0.004 is similar to normal glass spherules. However, their Ti/Si are much lower compared with CAT spherules.

## 4. Discussion

### 4.1 *Assessing the chemical composition of AMM and DSS glass spherules*

Glass spherule constitutes a large percentage in the micrometeorite collections, often that have undergone considerable melting with no visible phases

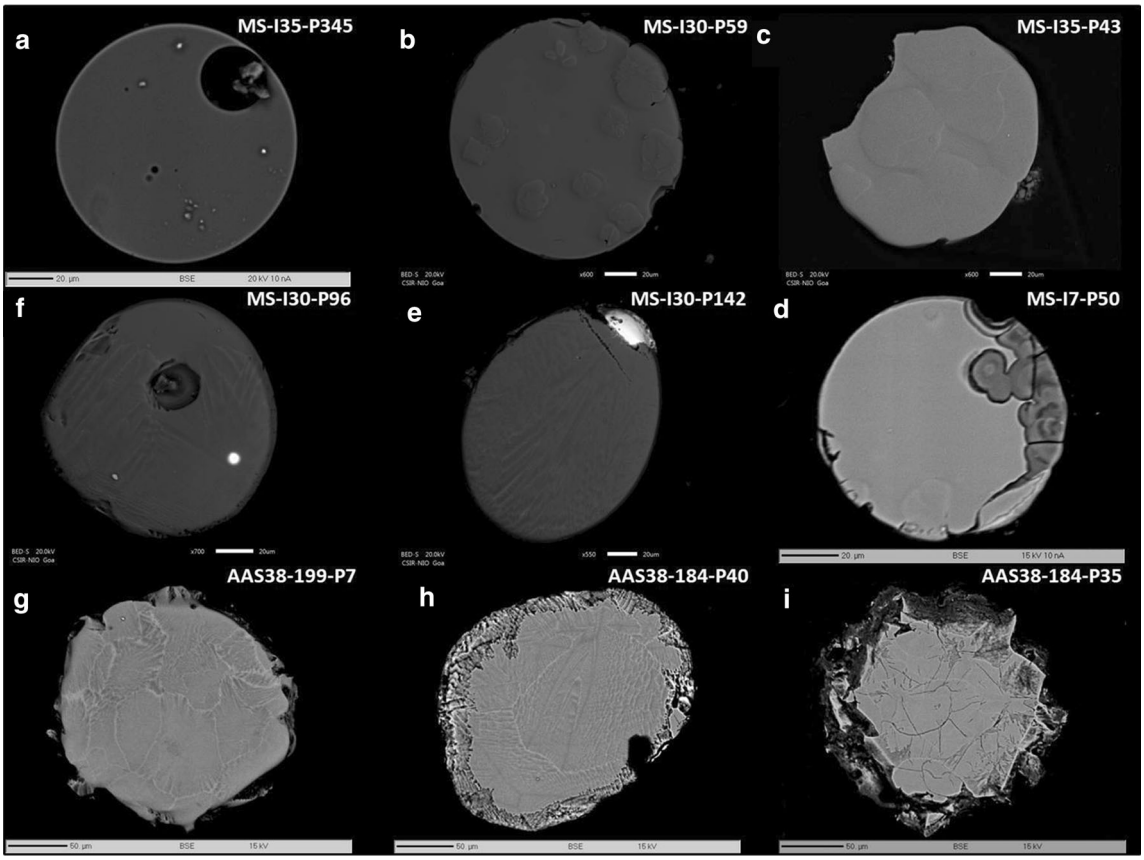


Figure 1. The representative SEM images of glass spherules from AMM (**a–d**) and DSS (**g–i**). (**b, c**) Normal glass spherules with radiating spherulitic centers inside. (**d**) Spherical glass spherule with a partial palagonite-like rim. (**e**) Oval glass spherules with protruding metal bead and display striated crystallization pattern inside. (**f**) Glass spherules containing small metal nuggets surrounded by spherulites. (**g**) Glass spherules with prominent scalloped features. (**h, i**) Scalloped glass spherules with considerable etched rims.

inside (Taylor *et al.* 2000; Genge *et al.* 2008). The heating led to the ablation of the volatile elements, thereby, altering the original composition of the precursors. Regardless of this, the earlier study carried out on stony spherules shows that most of the stony spherules still preserve their broad chondritic elemental ratios (Brownlee *et al.* 1997). Glass spherules from AMM, South Pole Water Well has shown that glass spherules are consistent with progressive evaporation of Fe in chondritic melt sequence, which is followed by CAT spherules (Taylor *et al.* 2000). However, the previous studies on glass spherules from DSS have shown that these spherules contain platinum group element nuggets and incipient pyroxene normative grains inside them (Rudraswami *et al.* 2012). But, these studies constitute a small quantity of glass spherules compared to the present study. Recently, investigation of glass spherule collected from the Transantarctic mountain have classified them into several chemical groups based on their optical characteristics and chemical composition, and REE pattern (Cordier *et al.* 2011).

Glass spherules reported here in chemical composition are similar to those in earlier investigation and appear to have sourced from similar parent bodies (Brownlee *et al.* 1997; Taylor *et al.* 2000; Cordier *et al.* 2011). Likewise, the bulk chemical compositional analysis performed for these glass spherules, normally show pyroxene normative glass. They have, average higher $SiO_2$ of $\sim$44 wt% and lower FeO of average $\sim$20 wt% (figure 2b) often without any metal inside compared to other S-type spherules. The glass spherules must have been molten droplets that were heated well above their liquidus temperature, and subsequently quenched due to an abrupt entry at sub-zero altitude. Under this condition, metal present in glass undergoes abrupt melting and density immiscibility segregation to form a metal bead that are unusual in other S-type spherules. The glass spherules are therefore become much more

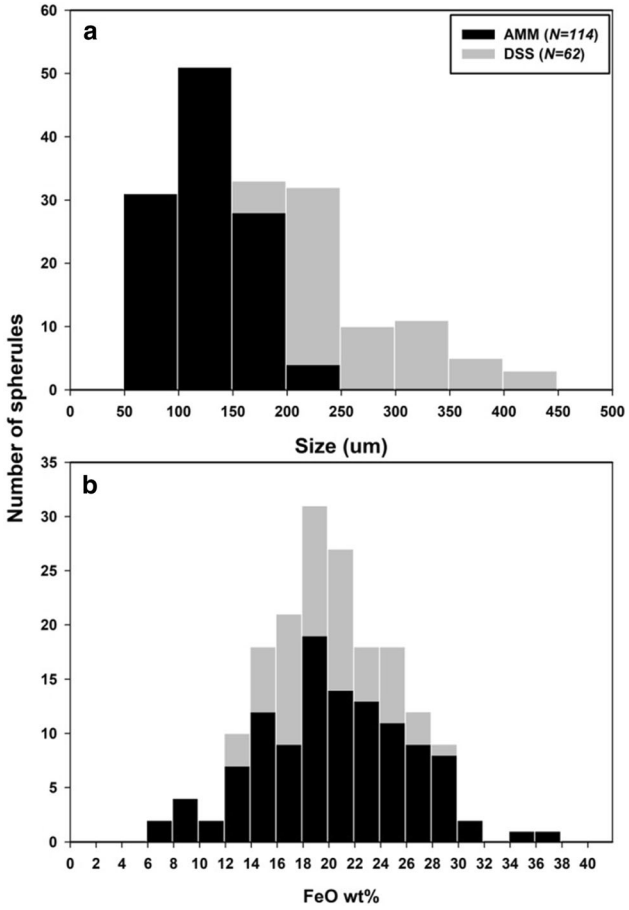


Figure 2. The histogram plots showing: (**a**) The size distribution of glass spherules obtained from AMM and DSS. (**b**) The glass spherules and their correspondent FeO wt%.

chemically altered compared to other S-type spherules. Nonetheless, their elemental ratio Fe/Mg *vs.* Fe/Mn is consistent and for most of them remained least affected displaying correlation with chondrites (figure 3d).

The bulk FeO in normal glass spherules is as minimum as ∼6 wt% noted to be far below when matched with the rest of the stony spherules, with the exception for CAT spherules and some Mg-rich olivine, and pyroxene containing relict-bearing spherules. Infact, FeO within glass spherules is responsible for altering most of its chemical composition followed by moderate $SiO_2$ and MgO from its parent precursors. This is primarily because FeO is very volatile sensitive at higher temperatures (Vondrak *et al.* 2008; Rudraswami *et al.* 2016). This is also apparent in Si–Mg–Fe systematics (figure 4a). The bulk chemical composition for normal glass spherules plotted within this ternary systematic tend to stand out to form a separate group from other stony spherules and in comparison are much more enriched in silica. For instance, the scoriaceous micrometeorites are expected to have formed at 1200°–1300°C with the least elemental Fe loss (Rudraswami *et al.* 2018a). This is because the scoriaceous matrices have faced partial melting which may have led low temperature volatile (anhydrite, carbonates and sulphides) to escape, while the rest of the major elements remains unaffected (Toppani *et al.* 2001). The Fe concentration in scoriaceous matrices could closely resemble the initial precursor composition, even though the scoriaceous micrometeorites are thought to originate from finer-grained materials that show correspondence with CI and CM carbonaceous chondrites (Rudraswami *et al.* 2018a).

The barred, porphyritic and cryptocrystalline spherules have undergone melting, but not to an extent that show slight depletion in Fe, however, Si and Mg loss is insignificant in this case. The porphyritic spherules among S-type represent less heated cosmic spherules that retain bigger nuclei for coarser olivine growth during crystallization. These spherules may have experienced temperatures well above 1300°C. During which much of the Fe, if it forms a metal due to reduction of silicate may contribute to crystallization as framboidal magnetites, otherwise Fe in silicate may be contributed to olivine overgrowths to form olivine crystals and olivine bars in porphyritic and barred spherules respectively, while the rest of Fe can account for ablative loss (Hashimoto *et al.* 1979).

The glass is expected to form at temperature >1700°C that can lead to metal to separate and form bead with tremendous elemental ablative loss (Hashimoto 1983; Rudraswami *et al.* 2012). The glass spherules that have undergone complete melting retained no nucleus for crystal growth, resulting into glass. The glass spherules in this regard suggest having suffered a substantial ablative loss that could be largely in the form of Fe, but also with significant Si and Mg loss. However, Si and Mg loss is not apparent in figure 4(a) as Fe loss is compensated by the enrichment of Si and Mg in the final glass. The glass spherules, thereby, show higher average $SiO_2$ of ∼44 wt% in relation to other S-type spherules. The FeO composition within CAT spherules is also significantly low that often also shows $SiO_2$ depletion (Taylor *et al.* 2000). The CAT spherules have therefore experienced much higher temperature in relation to normal glass spherules (Taylor *et al.* 2000; Cordier *et al.* 2011). This can be agreed upon by their consistent higher refractory oxide content, to some extent MgO also (figure 4a, b).

Table 1. *Major oxide composition of the selected representative AMM and DSS glass spherules.*

| Sample | $Na_2O$ | MgO | $Al_2O_3$ | $SiO_2$ | $P_2O_5$ | $SO_2$ | $K_2O$ | CaO | $TiO_2$ | $Cr_2O_3$ | MnO | FeO | CoO | NiO | Total |
|---|---|---|---|---|---|---|---|---|---|---|---|---|---|---|---|
| **AMM** | | | | | | | | | | | | | | | |
| MS-I4 P50 | 0.01 | 29.47 | 3.31 | 45.27 | 0.02 | 0.02 | – | 2.47 | 0.15 | 0.63 | 0.42 | 18.42 | 0.01 | 0.04 | 100.24 |
| MS-I4 P527 | – | 31.02 | 3.37 | 46.18 | – | 0.01 | 0.01 | 2.54 | 0.13 | 0.22 | 0.49 | 15.26 | 0.01 | – | 99.24 |
| MS-I3 P147 | 0.03 | 26.90 | 1.87 | 45.39 | 0.01 | 0.01 | 0.01 | 0.61 | 0.10 | 0.02 | 0.38 | 25.32 | 0.07 | 0.37 | 101.05 |
| MS-I3 541 | 0.01 | 26.95 | 3.33 | 43.41 | 0.03 | 0.01 | 0.01 | 2.48 | 0.18 | 0.55 | 0.44 | 21.48 | 0.03 | 0.11 | 99.00 |
| MS-I3 P899 | 0.01 | 28.88 | 2.87 | 45.12 | – | 0.01 | 0.01 | 1.97 | 0.15 | 0.49 | 0.39 | 18.35 | 0.02 | 0.02 | 98.23 |
| MS-I8 P12 | 0.01 | 33.15 | 2.20 | 45.81 | 0.02 | – | – | 1.52 | 0.09 | 0.30 | 0.39 | 15.93 | – | 0.05 | 99.48 |
| MS-I7 P496 | 0.01 | 27.41 | 5.72 | 40.68 | 0.03 | 0.01 | 0.01 | 2.41 | 0.19 | 0.16 | 0.21 | 23.11 | 0.01 | – | 99.93 |
| MS-I35 P29 | 0.01 | 31.36 | 1.62 | 47.84 | 0.15 | – | 0.01 | 2.43 | 0.20 | 0.70 | 0.31 | 13.93 | 0.01 | 0.09 | 98.63 |
| MS-I35 P785 | 0.01 | 23.84 | 2.49 | 44.28 | 0.06 | 0.02 | – | 2.88 | 0.14 | 0.40 | 0.44 | 23.83 | 0.06 | 0.54 | 98.98 |
| **Ca–Al Sph.** | | | | | | | | | | | | | | | |
| MS-I4 P678 | 0.00 | 28.65 | 5.81 | 43.92 | 0.03 | 0.01 | 0.01 | 4.46 | 0.22 | 0.07 | 0.05 | 16.31 | 0.01 | 0.01 | 99.57 |
| MS-I35 P39 | 0.42 | 20.42 | 4.03 | 44.59 | 0.08 | 0.01 | 0.07 | 4.98 | 0.16 | 0.29 | 0.41 | 21.76 | 0.00 | 0.13 | 97.35 |
| MS-I35 P632 | 0.31 | 15.13 | 14.00 | 45.54 | 0.01 | 0.01 | 0.02 | 4.92 | 0.05 | 0.22 | 0.12 | 17.05 | 0.10 | 0.12 | 97.56 |
| **DSS** | | | | | | | | | | | | | | | |
| AAS38-201-P186 | 0.03 | 30.47 | 1.53 | 46.99 | 0.06 | 0.01 | – | 1.15 | 0.05 | 0.62 | 0.49 | 17.26 | 0.03 | – | 98.69 |
| AAS38-199-P7 | 0.01 | 24.60 | 2.59 | 44.43 | 0.02 | 0.01 | – | 1.46 | 0.13 | 0.20 | 0.31 | 25.51 | 0.03 | 0.03 | 99.33 |
| AAS38-193-P60 | 0.01 | 24.48 | 2.27 | 44.95 | 0.02 | 0.01 | – | 1.85 | 0.16 | 0.58 | 0.33 | 24.72 | 0.04 | 0.13 | 99.55 |
| AAS38-170-P182 | 0.01 | 26.81 | 2.68 | 46.29 | 0.01 | 0.02 | – | 1.59 | 0.11 | 0.11 | 0.28 | 20.92 | 0.02 | 0.10 | 98.94 |
| AAS-62-28-P43 | 0.01 | 28.23 | 3.86 | 41.81 | 0.01 | – | 0.01 | 2.86 | 0.15 | 0.04 | 0.27 | 20.30 | 0.05 | 0.91 | 98.48 |
| AAS-62-06-P38 | – | 31.03 | 1.93 | 44.04 | – | 0.01 | 0.01 | 1.78 | 0.07 | 0.15 | 0.43 | 18.46 | 0.04 | 0.44 | 98.36 |
| AAS-62-11-P53 | 0.03 | 30.53 | 2.54 | 45.73 | 0.02 | – | – | 2.05 | 0.12 | 0.46 | 0.35 | 19.04 | 0.00 | 0.05 | 100.84 |
| AAS38-185-P1 | 0.02 | 33.11 | 3.05 | 41.65 | 0.02 | 0.01 | – | 2.82 | 0.15 | 0.02 | 0.23 | 18.06 | 0.02 | 0.01 | 99.17 |
| AAS-62-28-P112 | 0.02 | 28.99 | 3.30 | 43.48 | 0.01 | 0.02 | 0.01 | 1.96 | 0.13 | 0.17 | 0.23 | 21.27 | 0.03 | 0.09 | 99.67 |
| AAS-62-61-P114 | 0.02 | 29.29 | 3.76 | 41.03 | 0.02 | – | – | 2.51 | 0.15 | 0.01 | 0.22 | 21.74 | 0.01 | – | 98.76 |

Note: – below detection limit.

The Mg/Si ratio rises with progressive ablation that act as a tool in determining the ablation percentage. This is confirmed by heating experiments, to some extent also by numerical modelling (Hashimoto 1983; Rudraswami *et al.* 2015), thus allows us to estimate the amount of heating. In contrast, the Fe/Si ratio shows rapid decrease with increasing ablation percentage (Hashimoto 1983; Rudraswami *et al.* 2015). The Al/Si and Ca/Si ratio do not show much change at <50% ablative loss of particles beyond which they rise rapidly (Rudraswami *et al.* 2015). Similarly, the $TiO_2$ being incompatible and refractory oxide continues to saturate in final melt and can lead to increasing Ti/Si ratio. The CAT spherules exhibit the maximum Mg/Si and Ti/Si values and a lowest Fe/Si value that suggests to have formed at the highest temperatures in the cosmic spherule melt sequence. The glass spherules with low Fe/Si 0.1–0.9, high Mg/Si 0.7–1.8, and Ti/Si 0–0.006 suggest being the next-most heated particles after CAT during atmospheric entry heating.

The chemical composition of Ca–Al spherules identified here also compares well with those reported by Cordier *et al.* (2011); however, these are found to be much poor in $TiO_2$. The FeO ∼16–21 wt% within Ca–Al spherules is consistent with the normal glass spherules and their atomic Fe/Mg *vs.* Fe/Mn ratios fall within the chondritic region, which suggests to have derived from similar parent bodies in association with normal glass spherules. However, in this case, their formational condition or initial chemical aspects from normal glass spherules may vary. Within a progressive chondritic melt sequence CaO, $Al_2O_3$, and $TiO_2$ are refractory and incompatible oxides that continue to saturate in melt during crystallization process (figure 5). Therefore, they can accumulate in glass, either as a result of significant volatile elemental loss during the ablation process (Hashimoto 1983; Cohen *et al.* 2004) or, due to excessive utilization of susceptible silicate accomodating elements for crystal growth, thereby retains the residual melt concentrated with incompatible elements (Ca, Al, REE, etc,) (Connolly and Hewins 1991; Connolly *et al.* 1998; Varela *et al.* 2005, 2006; Usui *et al.* 2015). The former case explains the formation of glass and CAT spherules. However,

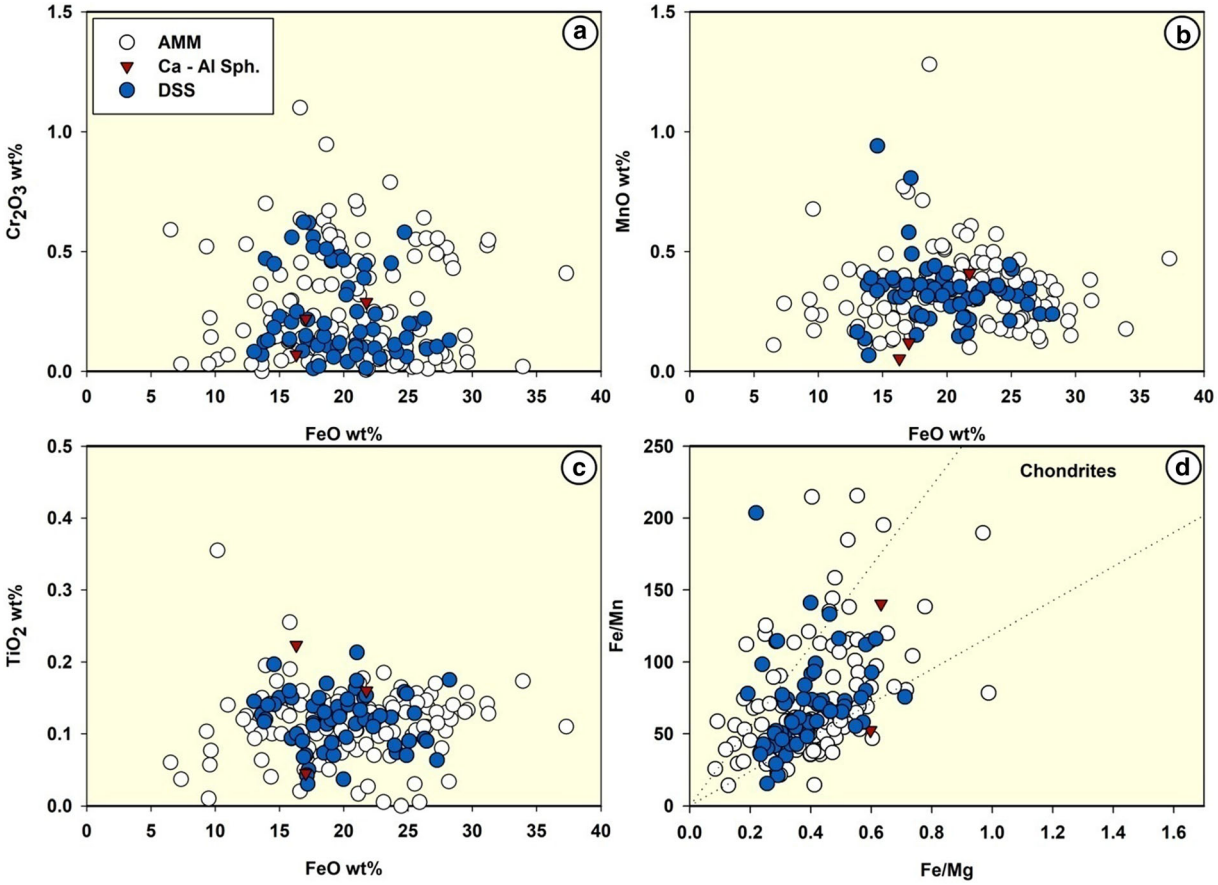


Figure 3. Minor oxide distribution plot of glass spherules. (**a**) $Cr_2O_3$ *vs.* FeO; (**b**) MnO *vs.* FeO; and (**c**) $TiO_2$ *vs.* FeO from AMM and DSS. (**d**) Elemental ratios plotted for glass spherules Fe/Mn *vs.* Fe/Mg (atomic) showing linkage with chondrites.

the latter is evident in groundmass made of glass found between olivine crystals in porphyritic spherules (Toppani *et al.* 2001). One of the recent studies on rare earth elements within Ca–Al spherules concludes to have suffered 80–90% of ablative loss far more exceeding than faced by CAT spherules (Cordier *et al.* 2011). Nevertheless, this can be argued on the fact that Ca–Al spherules still possess FeO within them and therefore highly unlikely to undergo 80–90% ablative loss, which does not comply with the experimental data (Hashimoto 1983; Rudraswami *et al.* 2016). In addition, Mg/Si ratios for Ca–Al spherules overlap with normal glass spherules even though they are enriched in refractory oxide. Higher CaO and $Al_2O_3$ can also arise from equilibration of subordinate Ca–Al rich phases with the background melt that can include feldspars, carbonates, maskylinite, etc. For this case, calcium–aluminium-rich inclusions (CAIs) are less probable (Grossman and Clark 1973). The CAIs are much enriched in $Al_2O_3$ and CaO, most of them are also stable at higher temperatures. Even if CAIs undergo melting, the residual melt should be enhanced much more in its constituent oxides than represented here, as they tend to remain in the melt (Beckett and Stolper 1994; Ivanova *et al.* 2017), which is not the case with these Ca–Al spherules. Nevertheless, they could also be much larger particles that can undergo much higher rapid ablation ∼80–90% due to their larger size and may still retain FeO in them with enriched CaO + $Al_2O_3$ and REE pattern in them.

Glass is expected to form when any superheated silicate melt cools rapidly. At this temperature, any metal existing within silicate will melt and segregate due to its immiscibility and density difference, which can later form a metal bead. In many cases, the empty cavity retained in glass spherules can be due to dislodged metal bead, but it can also be a hollow gas bubble trapped inside before rapid solidification during the entry process.

The deep-sea offers a tough environment for the glass spherules to survive. These can be ascertained from the fact that groundmass made of glass between olivine crystals in porphyritic spherules is

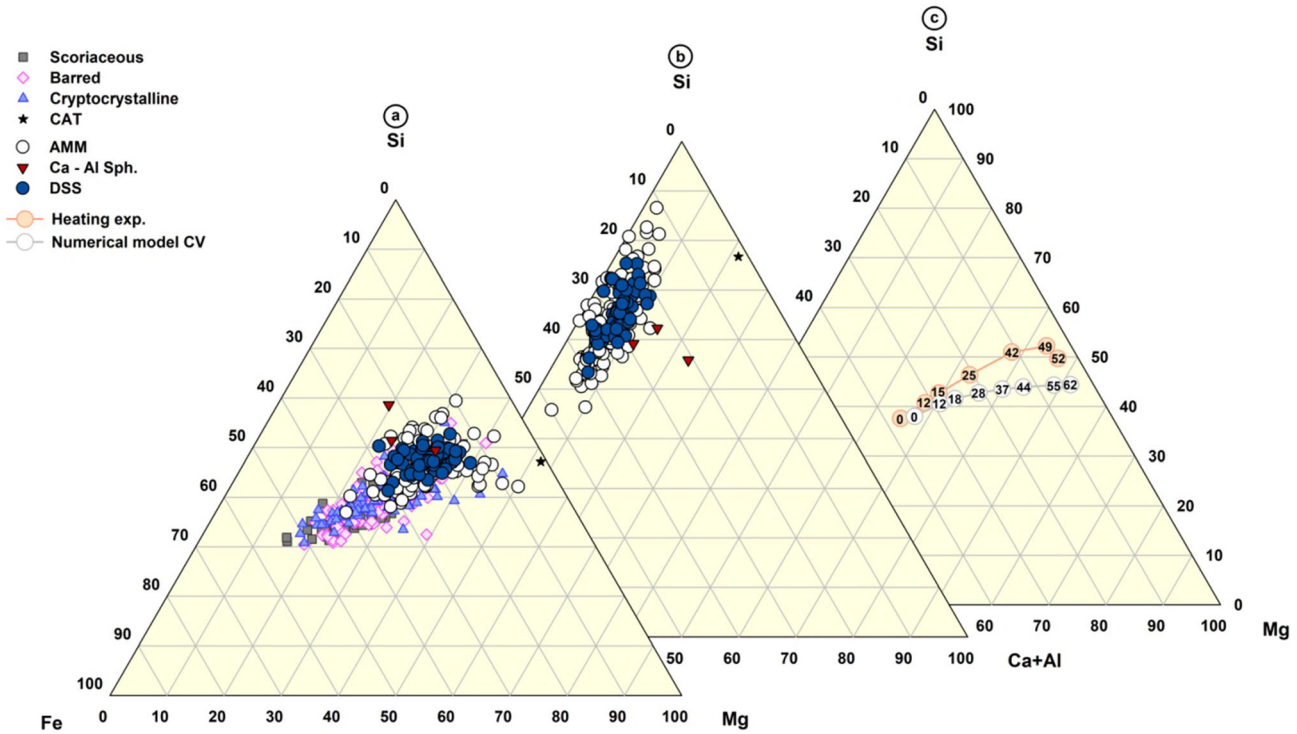


Figure 4. Ternary diagrams Mg–Fe–Si + (Al+Ca) (atomic) illustrating the bulk elemental composition of all glass spherules. (**a**) The Fe content of normal glass spherules is compared with barred, cryptocrystalline, CAT spherule, and scoriaceous micrometeorites (data for correlation sourced from Taylor *et al.* 2000; Rudraswami *et al.* 2015, 2018a). (**b**) The refractory element content of normal glass spherules with Ca–Al spherules in correlation with CAT spherule. (**c**) Heating experiment and numerical model data showing variation in elemental content relative to their percentages of ablation (data from Hashimoto 1983; Rudraswami *et al.* 2018a, b).

the first component to be etched out (Prasad *et al.* 2013) that is rich in Si, Ca, Al, and Fe. The chemical composition of glass spherules that is being enriched in silica and somewhat close to groundmass from porphyritic spherules may render glass spherules in deep-sea unstable. On the contrary, the Antarctica environment serves as an ideal condition for preserving glass spherules that show the least alteration and higher abundance in relation to DSS spherules.

### 4.2 *Atmospheric alteration of glass spherules*

Majority of the extra-terrestrial dust that bombards Earth's atmosphere undergoes ablative loss in atmospheric entry process (Love and Brownlee 1993). The abrupt changes extra-terrestrial particle experience due to atmospheric entry depend on particle chemical composition and initial atmospheric entry parameters, based on which particle attains peak temperature that determines the percentage of ablation (Rudraswami *et al.* 2015). To understand these changes the particle undergoes heating experiments, and numerical modelling has been attempted to understand their possible analogue meteorites (Hashimoto *et al.* 1979; Vondrak *et al.* 2008; Rudraswami *et al.* 2015). However, to simulate the exact entry conditions the particle has endured in the entry process in laboratory has been challenging. Nonetheless, previous studies conducted have helped us in understanding these chemical processes, e.g., Hashimoto (1983) used powdered rock sample and conducted heating experiment on it, whose chemical composition depicts chondrites. His work well emphasizes on chemical variation in chondritic melt that corresponds with crystallization and vapourization in an isothermal system (Hashimoto *et al.* 1979). This, however, contrasts with glass spherules that moreover have witnessed dynamic conditions. The numerical models have stressed its detail on chemical changes expressed by the particle to constrain upon atmospheric entry parameters (Vondrak *et al.* 2008; Rudraswami *et al.* 2015, 2016). Based on their results, it has been demonstrated that during atmospheric heating of particle, volatile elements are first to escape, followed by the siderophile (Rudraswami *et al.* 2016). Glass spherules are survived extraterrestrial dust

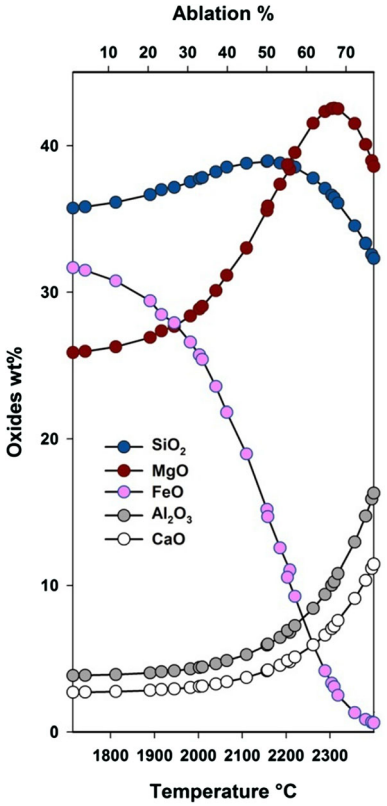


Figure 5. Variation in oxide composition wt% of $SiO_2$, MgO, FeO, $Al_2O_3$, and CaO with respect to temperature in °C and with corresponding ablation percentages for CV chondrite at entry velocity of 11 km/s for particle sizes between 100 and 500 μm at zenith angles 0°–70° (model data source Rudraswami *et al.* 2018a, b).

grains that have undergone rapid melting, upon flash heating and were completely molten liquid droplets in atmospheric entry process before being solidified. At this moment, mineral crystallization would only take place if enough nucleus and time persist, which is not possible at this stage. The FeO tends to be highly volatile at this stage, loss of FeO increases the $SiO_2$, MgO, CaO, $Al_2O_3$, and $TiO_2$ content in glass. Correspondingly, the Mg/Si ratio rises exponentially for micrometeorites up to, until ∼70% ablative loss, beyond this FeO wt% becomes totally depleted. In the midst of rapid FeO decreasing, $SiO_2$ shows a distinct effect facing temperatures >2200°C and having FeO dropped below 10 wt% (figure 5). The $SiO_2$ shows a moderate decrease at the loss of which Mg enriches in the residual melt, subsequently MgO also follows a similar trend. The CAT spherules closely resemble this case that appears to account for >50% of the ablative loss. The CaO, $Al_2O_3$, and $TiO_2$ act as refractory oxides and continues to increase in melt. This is confirmed by heating experiments to some extent supported by numerical modelling (Hashimoto *et al.* 1979; Rudraswami *et al.* 2016), and this, therefore allows us to estimate the amount of heating in glass spherules.

Results obtained from the numerical model and heating experiment is plotted in ternary systematic are compatible that follow similar trends (figure 4c). Cosmic spherules including glass spherules correlate well with these results. Moreover, the heating experiment appears to be more practically applicable with respect to, chemical changes pertaining to ablation effect over cosmic spherules, while the numerical model reasonably significant for determining the entry parameters. The numerical model calculation predicts that glass spherules have encountered temperatures above 1700°C (figure 5) with >20% of ablative loss (Rudraswami *et al.* 2012). These conclusions are well in agreement with Cordier *et al.* (2011) who estimated the ablation percent based on rare earth elements.

The calculation also suggests that larger size particles with higher entry velocity are likely to generate glass and CAT spherules as these parameters signify greater ablation. Overall based on these computed model for particles with carbonaceous chondritic composition in sizes of ∼300 to <400 μm entering at zenith angles 0°–50° under velocities of less than ∼16 km/sec support these conditions, as smaller particles and higher zenith angles 60°–80° show lower ablation percentage and particles beyond this size and velocity lose substantial mass (Rudraswami *et al.* 2018a, b). However, this window is much narrow for particles with the ordinary chondritic composition that holds valid mostly for the size of ∼200 μm and zenith angles 0°–60° (Rudraswami *et al.* 2018a, b).

## 5. Conclusion

Bulk chemical composition analyzed for AMM and DSS glass spherules are similar, however, their abundance in DSS is quite low. Glass spherules obtained from AMM have shown to contain more round spherules, compared with DSS that are irregular and relatively Fe enriched. This thereby puts a constraint on the micrometeorite sample collection technique and its efficiency. Detailed examination of the glass spherules chemical composition being explicitly composed of $SiO_2$ enriched glass with refractory elements and depleted in FeO content suggests extremely heated micrometeorites. The elemental behaviour within glass indicates the

large ablated portion mainly constitutes elemental Fe with subordinate Si and Mg. Based on the model calculation, the glass spherules appear to have suffered >20% of mass loss during atmospheric entry while the CAT spherules show >50% loss. The higher $Al_2O_3$ and CaO oxide content within Ca–Al spherules could be due to their larger size that have undergone excessive ablation or a result of equilibration of calcium and alkali rich phases as they retain FeO oxide in them that is similar to normal glass spherules. Glass spherules with preponderance of excessive glass chemistry and lack of mineral phases in them, disable us to know their exact precursors, however, their atomic ratios correlate with carbonaceous chondritic group.

## Acknowledgements

This research work is supported by the GEOSINKS, MOES-PMN, MOES-NCPOR, and the PLANEX project. We gratefully acknowledge the UGC-CSIR for their financial support. We thank Vijay Khedekar and Areef Sardar for providing technical support. We also thank the anonymous reviewers, for their comments and suggestions that have improved the quality of the manuscript. This is NIO's contribution no. 6672.

## Author statement

D Fernandes has carried out the main objective behind the manuscript, apart from sample collection, writing, and analysis. N G Rudraswami has supported for project funding, manuscript writing along with sample collection. M Pandey and M Kotha have supported during writing and reviewing the manuscript.

## References

Beckett J R and Stolper E 1994 The stability of hibonite, melilite and other aluminous phases in silicate melts: Implications for the origin of hibonite-bearing inclusions from carbonaceous chondrites; *Meteoritics* **29** 41–65.

Blanchard M B, Brownlee D E, Bunch T E, Hodge P W and Kyte F T 1980 Meteoroid ablation spheres from deep sea sediments; *Earth Planet Sci. Lett.* **46** 178–190.

Bradley J P, Sandford S A and Walker R M 1988 Interplanetary dust particles; In: *Meteorites and the Early Solar System*; (eds) Kerridge J F and Matthews, M S University Arizona Press, Tucson, pp. 861–898.

Brownlee D E, Joswiak D J, Love S G, Nier A O, Schlutter D J and Bradley J P 1993 Identification of cometary and asteroidal particles in stratospheric IDP collections; *24th Lunar Planet. Sci. Conf.,* pp. 205–206.

Brownlee D E, Bates B and Schramm L 1997 The elemental composition of stony cosmic spherules; *Meteorit. Planet. Sci.* **32** 157–175.

Cohen B A, Hewins R H and Alexander C M O D 2004 The formation of chondrules by open-system melting of nebular condensates; *Geochim. Cosmochim. Acta* **68(1)** 661–1675.

Connolly H C Jr and Hewins R H 1991 The influence of bulk composition and dynamic melting conditions on olivine chondrule textures; *Geochim. Cosmochim. Acta* **55** 2943–2950.

Connolly H C Jr, Jones B D and Hewins R H 1998 The flash melting of chondrules: An experimental investigation into the melting history and physical nature of chondrule precursors; *Geochim. Cosmochim. Acta* **62** 2725–2735.

Cordier C, Folco L, Suavet C, Sonzogni C and Rochette P 2011 Major, trace element and oxygen isotope study of glass cosmic spherules of chondritic composition: The record of their source material and atmospheric entry heating; *Geochim. Cosmochim. Acta* **75** 5203–5218.

Dohnanyi J S 1976 Sources of interplanetary dust: Asteroids; In: *Interplanetary dust and the zodiacal light* (eds) Elsasser H and Fechtig H (Berlin: Springer), vol. 48, pp. 187–206.

Dermott S F, Nicholson P D, Burns J A and Houck J R 1984 Origin of the Solar System dust bands discovered by IRAS; *Nature* **312** 505–509.

Flynn G N 1989 Atmospheric entry heating: A criterion to distinguish between asteroidal and cometary sources of interplanetary dust; *Icarus* **77** 287–310.

Genge M J, Engrand C, Gounelle M and Taylor S 2008 The classification of micrometeorites; *Meteorit. Planet. Sci.* **43** 497–515.

Gradie J C, Chapman C R and Tedesco E F 1989 Distribution of taxonomic classes and the compositional structure of the Asteroid Belt; In: *Asteroids II* (eds) Binzel R P, Gehrels T and Matthews M S; University Arizona Press, Tucson, pp. 316–335.

Grossman L and Clark S P Jr 1973 High-temperature condensates in chondrites and the environment in which they formed; *Geochim. Cosmochim. Acta* **37** 635–649.

Hashimoto A, Kumazawa M and Onuma N 1979 Evaporation metamorphism of primitive dust material in the early solar nebula; *Earth Planet. Sci. Lett.* **43** 13–21.

Hashimoto A 1983 Evaporation metamorphism in the early solar nebula-evaporation experiments on the melt $FeO–MgO–SiO_2–CaO–Al_2O_3$; *Geochem. J.* **17** 111–145.

Ivanova M A, Shornikov S I, Ryazantsev K M and Yakovlev O I 2017 Model calculations for evaporation of AOA and CAI melts: Implications for the bulk CAIs compositions of CV3 and CH–CB chondrites; *48th Lunar Planet. Sci. Conf.*, 1363p.

Kunz J, Bollinger K, Jessberger E K and Storzer D 1995 Ages of Australasian tektites; *26th Lunar Planet. Sci. Conf.,* pp. 809–810.

Love S G and Brownlee D E 1991 Heating and thermal transformation of micrometeoroids entering the Earth's atmosphere; *Icarus* **89** 26–43.

Love S G and Brownlee D E 1993 A direct measurement of the terrestrial mass accretion rate of cosmic dust; *Science* **262** 550–553.

Maurette M, Olinger C, Michel-Lévy M C, Kurat G, Pourchet M, Brandstätter F and Bourot-Denise M 1991 A collection of diverse micrometeorites recovered from 100 tons of Antarctic blue ice; *Nature* **351** 44–47.

Prasad M S, Rudraswami N G and Panda D K 2013 Micrometeorite flux on earth during the last ∼50,000 years; *J. Geophys. Res.* **118** 2381–2399.

Prasad M S, Mahale V P and Kodagali V N 2007 New sites of Australasian microtektites in the central Indian Ocean: Implications for the location and size of source crater; *J. Geophys. Res.* **112** E06007.

Rudraswami N G, Shyam Prasad M, Babu E V S S K, Vijaya Kumar T, Feng W and Plane J M C 2012 Fractionation and fragmentation of glass cosmic spherules during atmospheric entry; *Geochim. Cosmochim. Acta* **99** 110–127.

Rudraswami N G, Fernandes D, Naik A K, Shyam Prasad M, Carrillo-Sánchez J D, Plane J M C, Feng W and Taylor S 2018a Selective disparity of ordinary chondritic precursors in micrometeorite flux; *Astrophys. J.* **853** 38.

Rudraswami N G, Fernandes D, Naik A K, Shyam Prasad M and Taylor S 2018b Fine-grained volatile components ubiquitous in solar nebula: Corroboration from scoriaceous cosmic spherules; *Meteorit. Planet. Sci.* **53** 1207–1222.

Rudraswami N G, Shyam Prasad M, Dey S, Plane J M C, Feng W, Carrillo-Sánchez J D and Fernandes D 2016 Ablation and chemical alteration of cosmic dust particles during entry into the Earth's atmosphere; *Astrophys. J. Suppl. Ser.* **227** 15.

Rudraswami N G, Shyam Prasad M, Dey S, Plane J M C, Feng W and Taylor S 2015 Evaluating changes in the elemental composition of micrometeorites during entry into the earth's atmosphere; *Astrophys. J.* **814** 78.

Rudraswami N G, Fernandes D and Pandey M 2020 Probing the nature of extraterrestrial dust reaching the Earth's surface collected from the Maitri station, Antarctica; *Meteorit. Planet. Sci.* **55** 2256–2266.

Taylor S, Lever J H and Harvey R P 1998 Accretion rate of cosmic spherules measured at the South Pole; *Nature* **392** 899–903.

Taylor S, Lever J H and Harvey R P 2000 Numbers, types and compositions of an unbiased collection of cosmic spherules; *Meteorit. Planet. Sci.* **35** 651–666.

Toppani A, Libourel G, Engrand C and Maurette M 2001 Experimental simulation of atmospheric entry of micrometeorites; *Meteorit. Planet. Sci.* **36** 1377–1396.

Usui T, Jones J H and Mittlefehldt D W 2015 A partial melting study of an ordinary (H) chondrite composition with application to the unique achondrite Graves Nunataks 06128 and 06129; *Meteorit. Planet. Sci.* **50** 759–781.

Van Ginneken M, Genge M J, Folco L and Harvey R P 2016 The weathering of micrometeorites from the Transantarctic Mountains; *Geochim. Cosmochim. Acta* **179** 1–31.

Varela M E, Kurat G and Zinner E 2005 A liquid-supported condensation of major minerals in the solar nebula: Evidence from glasses in the Kaba (CV3) chondrite; *Icarus* **178** 553–569.

Varela M E, Kurat G and Zinner E 2006 The primary liquid condensation model and the origin of barred olivine chondrules; *Icarus* **184** 344–364.

Verniani F 1969 Structure and fragmentation of meteoroids; *Space Sci. Rev.* **10** 230–261.

Vondrak T, Plane J M C, Broadley S and Janches D 2008 A chemical model of meteoric ablation; *Atmos. Chem. Phys.* **8** 7015–7031.

Corresponding editor: N V Chalapathi Rao